RINOPOLYCRETE - TOWARDS A CEMENT-FREE AND FULLY RECYCLED CONCRETE

PROJECTO FCT

PTDC/ECI-COM/29196/2017

Recycled inorganic polymer concrete - Towards a cement-free and fully recycled concrete

(RInoPolyCrete)

Task 2 - Report 4

Results and discussion of the second experimental stage of Task 2: Pretreatment of MIBA and optimum NaOH and Na_2SiO_3 contents

March 2021

Financiamento FCT/POCI

Governo da República Portuguesa

União Europeia FEDER

FCT Fundação para a Ciência e a Tecnologia

MINISTÉRIO DA CIÊNCIA E DO ENSINO SUPERIOR Portugal

Table of contents

List of Tables

List of Figures

ACRONYMS

AAM	Alkali-activated materials
Al	Aluminum
C-(N-)A-S-H	Calcium (alkali) aluminosilicate hydrate gel
EDS	Energy dispersive X-Ray spectroscopy
FA	Fly ash
ICP-OES	Inductively coupled plasma - optical emission spectrometry
MIBA	Municipal solid waste incinerator bottom ash
MSW	Municipal solid waste
Na_2SiO_3	Sodium silicate
NaOH	Sodium hydroxide
N-A-S-H	Sodium aluminosilicate hydrate gel
pH	Hydrogen potential
XRD	X-ray diffraction
XRF	X-ray fluorescence

1 Introduction

The alkaline activation process of waste with a high content of amorphous aluminosilicates generates a polymerization reaction producing the gels N-A-S-H or C-(N-)A-S-H (Khale & Chaudhary, 2007; Myers, Bernal, & Provis, 2014), which show mechanical properties similar or even greater than those of conventional cement hydration products.

The selection of the waste that will be subjected to this process is a key task since the quality of the activation depends on the characteristics of the source material. Precursors such as fly ash (FA) are widely known for their high availability of amorphous aluminosilicates, which leads to an activated material with excellent mechanical properties and durability, being the reason why some have called it the cement of the future (Bocullo, Vaičiukynienė, Gečys, & Daukšys, 2020; Fang, Ho, Tu, & Zhang, 2018; Farhan, Sheikh, & Hadi, 2019).

Municipal solid waste incinerator bottom ash (MIBA) is of interest due to its continuous generation from the kerbside collection of municipal solid waste (MSW) (Blasenbauer et al., 2020; Xuan, Tang, & Poon, 2018), contrary to the phasing out of FA from coal power plants.

Research has been recently carried out related to the optimization of the variables that influence the alkaline activation process of MIBA. Some of these studies emphasized the need for pretreatment of the material associated involving the release of hydrogen from the reaction of metallic aluminium in an alkaline medium (Maldonado-Alameda, Giro-Paloma, Svobodova-Sedlackova, Formosa, & Chimenos, 2020; Mary Joseph, Snellings, Nielsen, Matthys, & De Belie, 2020; Tian, Rao, León-Patiño, & Song, 2020), the optimization of the alkaline activator (Guodong Huang, Yang, Sun, et al., 2020), the influence of amorphous silica available for activation (G. Huang et al., 2019), the influence of the curing method (Guodong Huang, Ji, Zhang, Li, & Hou, 2018), among others. Nevertheless, it is considered that there is a great gap in the literature regarding the valorization of MIBA alkali-activated materials and other construction applications.

This report presents the results of the experimental campaign in report 2.3, analyzing exclusively the Na_2O/binder ratio and the silicon oxide/sodium oxide (SiO_2/Na_2O) ratio on the

alkali activation of MIBA (Valorsul, MSW thermal power plant) and FA (Energias de Portugal, EDP at Sines Power Plant) as precursors.

2 Materials and methods

The methodology, materials, mixing process and test methods are described in report 2.3.

3 Results and discussion

3.1 Characterization of the waste precursors

3.1.1 X-ray fluorescence

Table 1 shows the chemical composition of MIBA (produced in January 2019) and FA used in the present investigation. The data show that the sum of the oxides SiO_2 + Al_2O_3 + Fe_2O_3 correspond to 88.65 and 64.28 for FA and MIBA, respectively. When comparing these values with the ASTM C618-5 (Materials, 2017), it is possible to classify FA as type F, in which the sum of the oxides has a minimum established value of 70%. In the case of MIBA, the classification as per ASTM indicates that the waste can be classed as type C fly ash, since the value exceeds the established limit of 50% for the sum of the oxides. According to the literature, 66% of MIBAs comply with this limit (Lynn, Dhir, & Ghataora, 2017).

Table 1 - Chemical composition of raw materials, FA and MIBA (% by mass)

Materials	FA (%)	MIBA (%)
Al_2O_3	25.48	8.82
CaO	2.28	18.29
Fe_2O_3	6.90	6.68
K_2O	2.74	1.59
MgO	1.83	4.0
Na_2O	1.29	6.53
SiO_2	56.27	48.78
SO_3	0.80	1.36
Cl^-	0.0	0.0

Figure 1 shows the ternary diagram SiO_2 - Al_2O_3 - CaO, which correspond to the main oxides directly responsible for the generation of oligomers that give rise to the N-A-S-H or C-(N-)A-S-H products, once they are dissolved in alkaline environments. It can be observed that MIBA samples generated in the months of September 2018, October 2018, December 2018 and

January 2019 are similar to each other and to samples from other studies (Cristelo et al., 2020; Guodong Huang, Yang, Sun, et al., 2020). Finally, the figure shows the typical areas for each pozzolanic addition (Lothenbach, Scrivener, & Hooton, 2011), confirming the previously established classification for the waste of the present study.

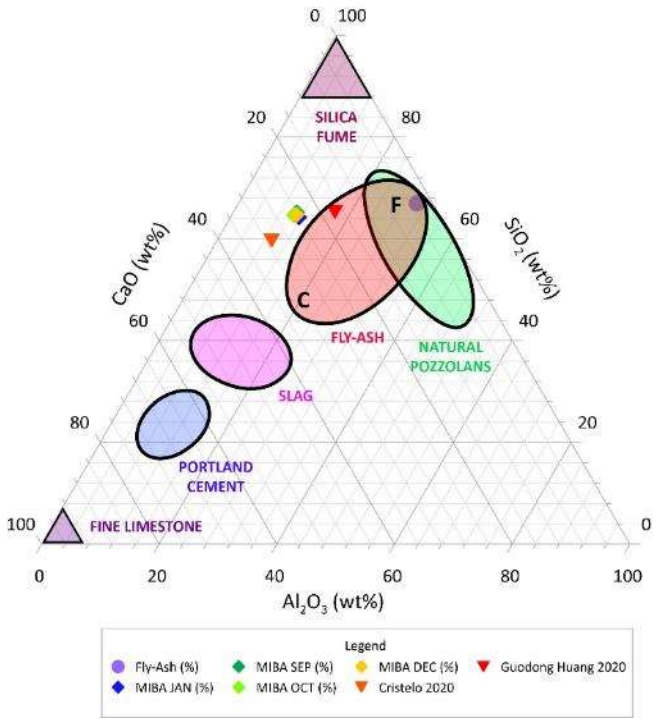

Figure 1 - Ternary diagram of CaO-Al_2O_3-SiO_2 content

3.1.2 X-ray diffraction

Figure 2 corresponds to the X-ray diffraction (XRD) results of the MIBA samples used in the present study. The crystalline phases observed are quartz (SiO_2), calcite ($CaCO_3$), magnetite ($Fe^{2+}Fe^{3+}2O_4$), fayalite ($(Fe^{2+})_2SiO_4$), magnesian ($MgCO_3$), microcline ($KAlSi_3O_8$), magnesium phosphate ($Mg_3(PO_4)_2$), sodium calcium iron phosphate and anhydrite ($CaSO_4$).

This research is consistent with other articles where similar minerals were found (Bayuseno & Schmahl, 2010; Wei et al., 2014), therefore, the results of this report are consistent with the literature.

On the other hand, Figure 3 corresponds to the XRD for FA sample used in the present study. The crystalline phases observed are quartz (SiO_2), lime (CaO), maghemite ($Fe^{3+}2O_3$) and mullite. Mineralogical characterization of FA is similar to that reported by other authors (Cho, Yoo, Jung, Lee, & Kwon, 2017; Rashad & Zeedan, 2011).

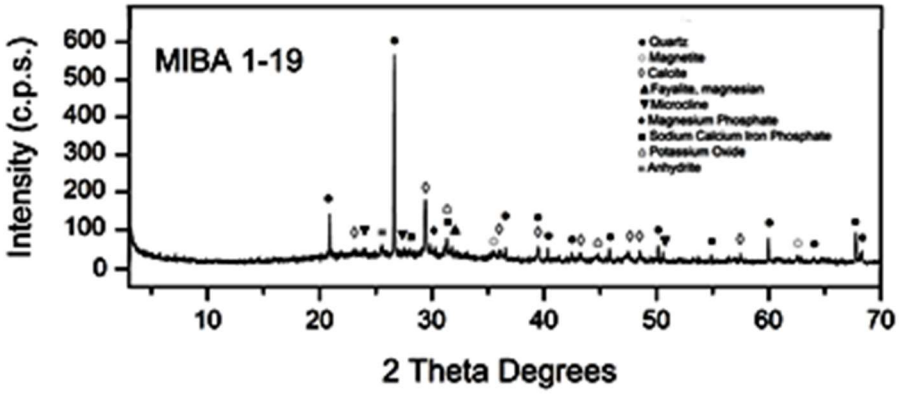

Figure 2 - XRD pattern of MIBA

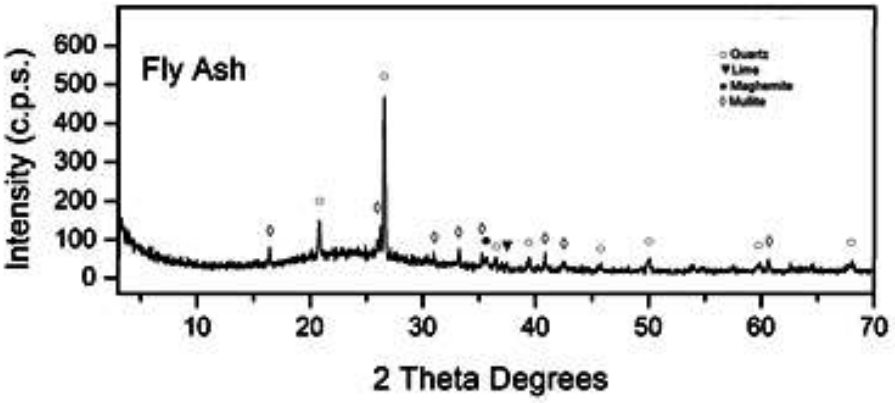

Figure 3 - XRD pattern of FA

3.1.3 pH

Hydrogen potential test was carried out using a digital pH measurement instrument HACH brand. The procedure for pH determination in soils was based on ASTM D4972 (Materials, 2019). MIBA and FA presented values of 9.50 and 10.70, respectively, which indicates the alkaline nature of both precursors. High pH values are key in the alkaline activation process.

3.1.4 Quantification of metallic aluminium in MIBA

The chemical reaction to produce gaseous hydrogen from metallic aluminium and sodium hydroxide corresponds to equation 1A. Stoichiometric quantities (atomic and molecular weights in grams) are presented in equation 1B.

$$2Al^0 + 2NaOH + 6H_2O \rightarrow 2NaAl(OH)_4 + 3\,H_2\uparrow \qquad \text{Eq. 1A}$$

$$54g + 80g + 108\,g \rightarrow 236g + 6g\uparrow \qquad \text{Eq. 1B}$$

From the stoichiometric quantities, it was determined that 0.11 g of $H_2\uparrow$ were produced per gram of aluminium consumed (Eq. 2).

$$g\ H_2\uparrow = 1\ \text{g Al°} \times \frac{6\ g\ H_2\uparrow}{54\ g\ Al°} = 0{,}11\ g \qquad \text{Eq. 2}$$

From the reaction of 0.1 g of metallic aluminium with a 2.5 M NaOH solution (excess reagent), the volume of water displaced by the hydrogen gas produced was measured experimentally in an inverted test tube, which was connected through a glass tube to a three-nozzle balloon (Figure 4a). The theoretical value at which the error was calculated corresponds to 143.03 ml.

Three runs were performed to determine the average and calculate the error. The temperature at which the reaction was carried out was 43 °C, and this heat is due to the exothermic reaction of NaOH in water.

The density of the hydrogen at 43 °C and 1 atm. of pressure is 0.0766 kg/m^3 ("Engineering ToolBox. Hydrogen - Density and Specific Weight.," 2018). From this property and the mass of hydrogen produced by each gram of aluminium (Eq. 3), it was possible to determine the theoretical volume of hydrogen generated.

$$v = \frac{m}{\rho}; \quad v_{H_2} = \frac{0{,}11\ g}{0{,}0000766\ g/ml} = 1436{,}03\ ml \qquad \text{Eq. 3}$$

One gram of metallic aluminium generates 1.436 litres of H_2. Table 2 shows the measurements made in triplicate for 0.1 g of pure metallic aluminium.

Table 2 - H_2 release by 0.1 Al°

Vi (ml)	Vf (ml)	Vexp (ml)
10	142	132
30	156	126
28	164	136
Average		131.33
Std.Dev.		5.03
Error		8%

To quantify of metallic aluminium in MIBA, the test was carried out with 30 g of this precursor and 800 ml of a 2.5 M NaOH solution. The results are presented in Table 3.

Table 3 - H_2 release by 30 g of MIBA

Vi (ml)	Vf (ml)	V exp (ml)
50	218	168
41	200	159
23	172	149
Average		158.67
Std.Dev.		9.50

Using the density, the milligrams of hydrogen present in 158.67 ml of the gas were determined (Eq. 4):

$$v\ x\ \rho = m; \quad 158.67ml\ x\ 0{,}0000766\frac{g}{ml} = 0.01215\ g = 12.15\ mg \qquad \text{Eq. 4}$$

Where v corresponds to the volume in ml, ρ is the density in g/ml and m, the mass in mg. Using the stoichiometries weights, in the equation. 5, the amount of metallic aluminium that produces this quantity of hydrogen is determined.

$$g\ Al° = 0.01215\ \text{g}\ H_2 \uparrow\ \text{x}\ \frac{54\ g\ Al°}{6\ g\ H_2 \uparrow} = 0.1640\ g\ Al° \qquad \text{Eq. 5}$$

Therefore, in 30 g of MIBA there are 164.025 mg of metallic aluminium, and it can be concluded that there are 5.46 g of Al/kg of MIBA and that this aluminium in contact with an

excess NaOH solution produces 7.91 L of H_2 ↑/kg of MIBA. Figure 4b shows the relationship between the hydrogen released by MIBA and time in minutes.

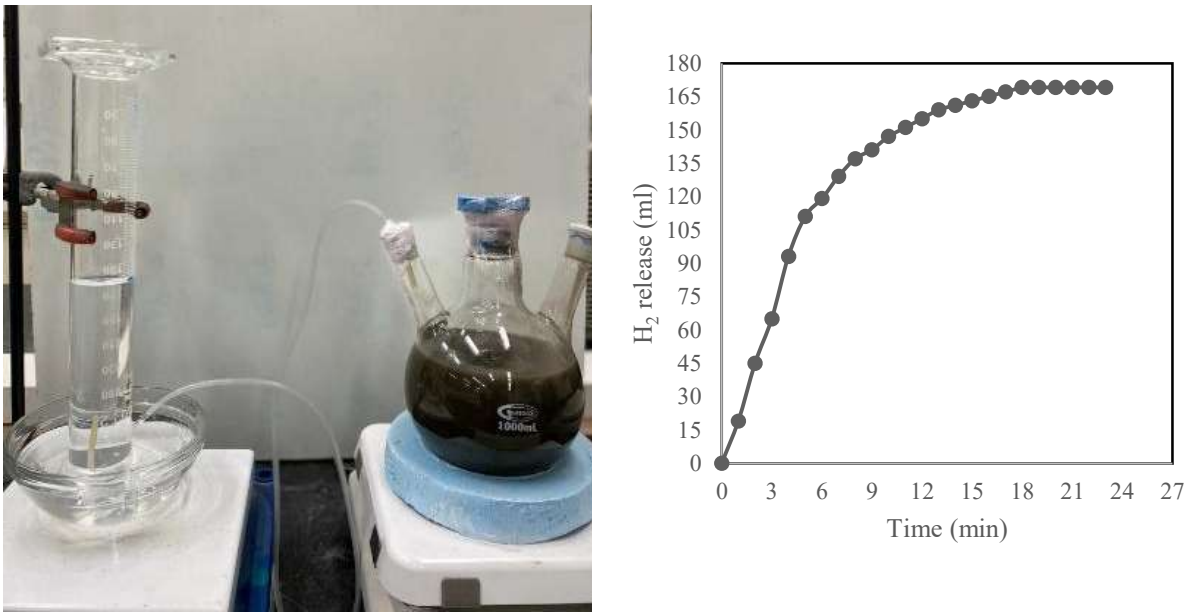

Figure 4 - Quantification of metallic aluminium in MIBA: (a) experimental setup (b) H_2 released by MIBA over time

3.1.5 Pozzolanic activity index

In the modified Chappelle test determined by titration with 0.1 M HCl, the content of CaO consumed by the reactive phases present in FA were determined during 16 h of reaction at 90 ± 5 °C of 2 g CaO grade laboratory and 1 g of the by-product diluted in decarbonated water. The reactions presented in the titration are the following (equations 6 and 7):

$$CaO + 2HCl \rightarrow CaCl_2 + H_2O \quad \text{Eq. 6}$$

$$Ca(OH)_2 + 2HCl \rightarrow CaCl_2 + 2H_2 \quad \text{Eq. 7}$$

Therefore, it is possible to calculate the mg CaO / g of by-product (Técnicas, 2010) (equation 8):

$$\frac{mg\ CaO}{g\ by-product} = \frac{28\ x\ (v_3 \times m_3 - v_2) \times F_c \times 2 \times 2}{m_4 \times m_3 \times m_2}\ x\ 1.32 \quad \text{Eq. 8}$$

Where m_2 is the mass of the pozzolanic material expressed in grams, m_3 is the mass of CaO mixed with pozzolanic material, m_4 is the mass of CaO in the blank test, v_2 is the HCl consumed by the sample (ml); v_3 is HCl consumed by the blank (ml); Fc, the correction factor for a 0.1 M solution of HCl.

Through the Chappelle test, a value of 1513.4 mg of CaO per g of FA was obtained, which is higher than the minimum limit, 330 mg CaO/g of addition established by Raverdy et al. (Hoppe Filho, 2017; Raverdy, Brivot, Paillere, & Dron, 1980). Nevertheless, it should be noted that, according to the standard NBR 15895 (Técnicas, 2010), the Chapelle test is not recommended for samples with high Ca content. Evaluating the amorphous aluminosilicates phases in MIBA should be made by means of inductively coupled plasma optical emission spectrometry (ICP - OES) (Kuenzel & Ranjbar, 2019; Liu, Sidhu, Chen, & Yang, 2018).

3.2 MIBA pretreatment

In order to avoid the production of H_2 in AAM mixes, it was established that a pretreatment to MIBA was required. In this treatment, the NaOH concentration varied depending on the alkaline activator for a fixed reaction time of 24 hours. The main reaction that takes place in the pretreatment is the following (Equation 9):

$$2Al + 2NaOH + 6H_2O \rightarrow 2NaAl(OH)_4 + 3\,H_2\uparrow \qquad \text{Eq. 9}$$

In this reaction, ~5.46 grams of aluminium are oxidized for each kg of MIBA by an exothermic oxidation reaction (-16.3 kJ/g Al°).

In the present work, the heat released in the reaction of dissolving NaOH in water was used as catalyst for the release of hydrogen (46.2 kJ/mol at a NaOH concentration of 1 mol/L). At a higher concentration of alkali, the reaction of metallic aluminium will be favoured due to increased heat input (Mary Joseph et al., 2020). Rosenband and Gany (Rosenband & Gany, 2010) studied the behaviour of the release of hydrogen associated with the reaction of aluminium with water at various temperatures, confirming that, when the water reached 74 °C, the reaction occurred in a shorter time than when they used water at 50 °C. In the present work, the reaction temperature of the NaOH solution used to treat MIBA was between 80 °C and 83 °C.

NaOH suffers a complete dissolution in water and, therefore, the concentration of the solute will be equal to the concentration of the ions in the aqueous medium (Equation 10):

$$NaOH \rightarrow Na^{+} + OH^{-} \quad \text{Eq. 10}$$

The concentration of NaOH was determined experimentally through the titration of the alkaline solution with hydrochloric acid (HCl) and using phenolphthalein as an indicator. The chemical reaction that takes place is as follows (Equation 11):

$$NaOH + HCl \rightarrow NaCl + H_2O \quad \text{Eq. 11}$$

The experimental molarity of the base was determined through the following formula (equation 12):

$$M_{NaOH} = \frac{V_{HCl} \times M_{HCl} \times \#H^{+}_{given}}{V_{NaOH}} \quad \text{Eq. 12}$$

Where M_{NaOH} is molarity of sodium hydroxide, V_{NaOH} is the volume of sodium hydroxide solution in titration (50 ml), M_{HCl} is the molarity of hydrochloric acid (2 M), V_{HCl} is the consumed volume of hydrochloric acid solution and $\#H^{+}_{given}$ is the number of hydronium ions released in the acid-base neutralization reaction.

In the pretreatment of each family, MIBA was mixed with a solution containing the amount of NaOH needed for each corresponding mix. After the treatment, the Na_2SiO_3 was added (when applicable) to the rest of materials to produce the AAM mixes. Table 4 shows the theoretical vs. experimental OH^- concentration. Note that, although the first column also presents the notation equivalent to the SiO_2/Na_2O ratio (e.g. 4/1.0 means Na_2O/binder / SiO_2/Na_2O ratio), the solution used for this test only contains NaOH. Firstly, this experiment showed a small error thus inferring the precision and reproducibility of the test. For a Na_2O content of 4%, as the SiO_2/Na_2O ratio increased to produce AAM, the concentration of OH^- decreased. This trend, however, reversed for higher contents of Na_2O. Since the total amount of water was divided into added tap water and that from the Na_2SiO_3 solution, increasing the Na_2O content

meant lower amount of additional water and thus a higher concentration of NaOH without increasing the amount of this component. For example, comparing the M4/0 and M15/1.0 mixes, which are on opposite ends, the NaOH solution of M4/0 contains 51.61 g NaOH / 1000 g MIBA and 505.80 g water / 1000 g MIBA, while the extreme M15/1.0 It is composed of 134.92 g NaOH / 1000 g MIBA and 133.8 g water / 1000 g MIBA. This means that, even though the concentration of the solution increases with the Na_2O/binder ratio, the amount of water available for pretreatment decreases, which leads to insufficient enveloping of the entirety if MIBA particles ending up with unreacted aluminium in the precursor.

Table 4 - Experimental determination of the content of OH^- ions in mixes

Mix	NaOH/MIBA (g / 1000 g)	Water/MIBA (g / 1000 g)	Theoretical molarity of NaOH	Theoretical volume of consumed HCl (ml)	Real volumen of consumed HCl (ml)	Experimental concentration of OH^-	Error
4/0	51.61	505.80	2.43	60.50	61.0	2.44	0%
4/0.5	43.80	456.08	2.30	57.10	57.2	2.29	0%
4/1.0	35.94	406.43	2.12	52.75	51.4	2.06	3%
4/1.5	28.15	356.74	1.90	47.27	47.2	1.89	1%
4/2.0	20.36	307.05	1.61	39.96	39.4	1.58	2%
6/0	77.42	505.80	3.57	88.73	88.4	3.54	1%
6/0.5	65.70	431.25	3.55	88.33	86.2	3.45	3%
6/1.0	53.93	356.71	3.53	87.71	85.8	3.43	3%
6/1.5	42.23	282.18	3.50	86.89	84.4	3.38	3%
6/2.0	30.53	207.62	3.44	85.46	83.6	3.34	3%
8/0	103.23	505.80	4.66	115.71	113.0	4.52	3%
8/0.5	87.59	406.40	4.89	121.60	119.4	4.78	2%
8/1.0	71.95	307.01	5.28	131.17	128.6	5.14	3%
8/1.5	56.30	207.61	6.01	149.47	145.0	5.80	4%
8/2.0	40.66	108.22	7.99	198.46	192.6	7.70	4%
10/0	129.03	505.80	5.70	141.55	146.8	5.87	3%
10/0.5	109.50	381.53	6.32	157.14	152.6	6.10	3%
10/1.0	89.94	257.29	7.51	186.56	183.0	7.32	2%
10/1.5	70.38	133.10	10.59	263.21	257.8	10.31	3%
15/0	193.55	505.80	8.11	201.54	210	8.40	4%
15/0.5	164.23	319.42	10.35	257.33	249.8	9.99	3%
15/1.0	134.92	133.08	17.17	426.77	416.8	16.67	3%

Figure 5 presents the volumetric ratio of NaOH solution per MIBA during the material's pretreatment and the molarity of the solution. The results suggest that the concentration of the hydroxyl ion (OH^-) is higher when the Na_2O/binder ratio increases, since the amount of NaOH required in the pretreatment stage is progressively increased (from 1.61 M for M4/2.0 mix to 17.17 M for M15/1.0 mix). On the other hand, as mentioned, by increasing the SiO_2/Na_2O ratio, the amount of water to be added to prepare the sodium hydroxide solution used in the pretreatment decreases. In the mix design of the present investigation, it was established that the parameter water/precursor ratio is constant (i.e. 0.5) and the sodium silicate used contained 65.6% of water. This previously set condition caused the NaOH solution/MIBA ratio to decrease. For this reason, the volume of some of the solutions (especially those to contain Na2SiO3) was not enough to wet the entire amount of MIBA during the pretreatment stage and thus complete oxidation of the aluminium was not attained within the 24 hours.

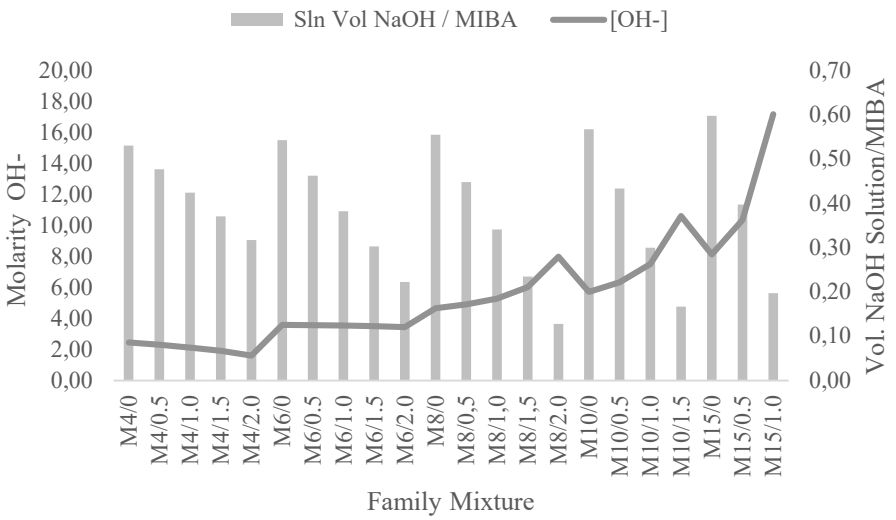

Figure 5 - Concentration and volume of the alkaline solution in the MIBA pretreatment

3.3 Fresh-state properties

3.3.1 Density

The determination of bulk density in the fresh state was carried out according to EN 1015-6 (EN, 1999). The fresh density for all mixes reveals that all values vary between 1.459 g/cm^3 and 2.144 g/cm^3 for families M15/1.0 and M4/0.5, respectively (Figure 6). Jinyoung et al.

(Kim, An, Nam, & Tasneem, 2016) determined the density in the fresh state for cement pastes with MIBA as mineral addition and reported values ranging from 1.718 g/cm^3 to 1.790 g/cm^3, corresponding to a paste with 30% replacement. Likewise, for the control paste, a slightly higher density was reported (1.878 g/cm^3), thus confirming the decrease in density caused by MIBA. The density of the MIBA used in this experimental campaign has a value of 2.704 g/cm^3, which is lower than the density of Portland cement (3.15 g/cm^3), which justifies the density decrease. It was observed that the Na_2O/binder ratio does not have a significant impact on the fresh density of the families. However, increasing the SiO_2/Na_2O ratio led to notable decrease in density (Figure 7), where foaming was observed in the mixes in the fresh state. The decrease in this property is associated with the reaction of metallic aluminium that was not oxidized in the MIBA pretreatment. Eliche Quesada et al. (Eliche-Quesada, Ruiz-Molina, Pérez-Villarejo, Castro, & Sánchez-Soto, 2020) used aluminium powder as a foaming agent to obtain a highly porous geopolymer for insulating material, using NaOH and Na_2SiO_3 as alkaline activators. It is expected that, whenever MIBA contains unoxidized aluminium after the pretreatment stage, the remaining amount acts as a foaming agent. Regarding the density in the hardened state at 28 days, it is observed that the values varied between 1.52 g/cm^3 and 2.05 g/cm^3 for the families M8/0.5 and M4/0, respectively, with a trend similar to the fresh density.

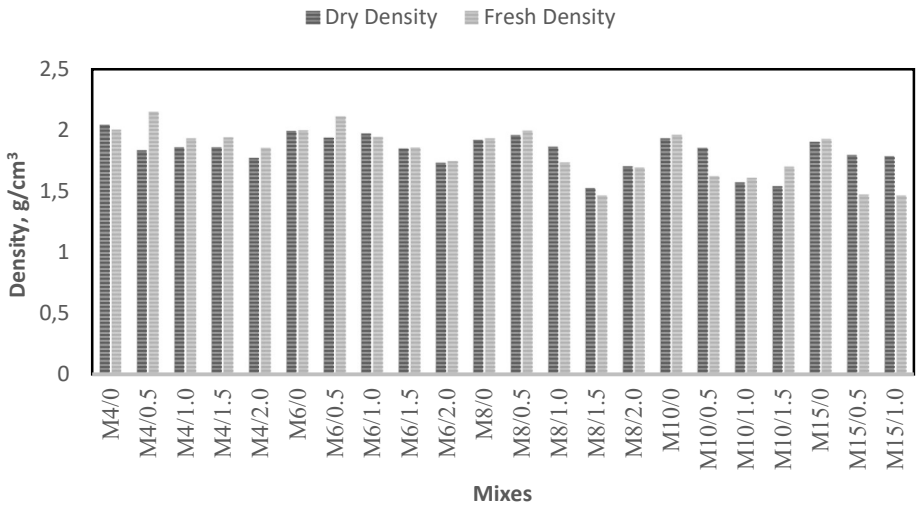

Figure 6 - Density in the fresh state and dry state of MIBA mortars

Figure 7 - Foaming MIBA in fresh state

The density in the fresh- and hardened-state at 28 days of the mixes made with FA as precursor is shown in Figure 8. The fresh-state density values varied between 1.793 g/cm^3 for the F4/2.0 family and 2.492 g/cm^3 for the F6/0.5 family. In general, the density values have an average of 2.223 g/cm^3 with a standard deviation of 0.114, which indicates that there is not a considerable scatter.

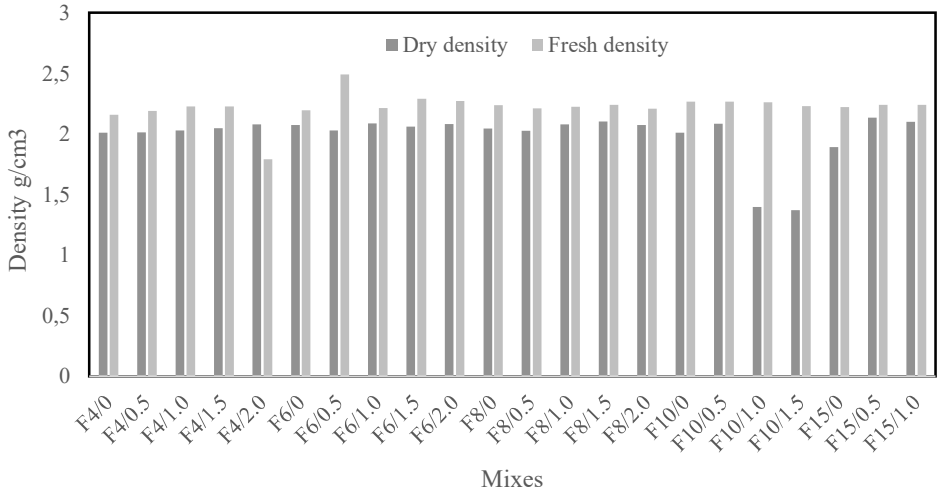

Figure 8 - Density in the fresh and dry state of FA mortars

3.3.2 Workability

The workability test was carried out according to EN 1015-3 ("BS EN 1015-3 Determination of

consistence of fresh mortar (by flow table)," 1999). Figure 9 shows the values obtained for the workability of mortars made with MIBA. When increasing the SiO_2/Na_2O ratio, the families with Na_2O/binder of 4% and 6% presented a dry consistence. Those with a Na_2O/binder ratio of 8% and with an increasing SiO_2/Na_2O ratio presented a high initial workability that degraded in a short period of time (Figure 10); therefore, it was not possible to determine this property for all mixes. These findings are in accordance with that reported by Puertas (Puertas, Varga, & Alonso, 2014). In this research, the rheology of alkali-activated mixes was evaluated, having slag as a precursor. The author observed that, when using NaOH and waterglass as alkaline activators, the mix in the fresh state behaved like a Herschel-Bulkley model fluid, concluding that this behaviour could be associated with the formation of C-S-H primary gels and thus loss of workability. Finally, other authors confirm the behaviour found (Palacios, Alonso, Varga, & Puertas, 2019).

The mixes with the highest workability are those made with the lowest ratios of Na_2O/binder and SiO_2/Na_2O (i.e. M4/0). Mixes M6/0, M8/0, M10/0 were classified as plastic mortars according to the standard (140 mm < spread < 200 mm), M15/0 was classified as a dry mortar. The results show that increasing the concentration of Na_2O decreases the workability. It has been established that the viscosity of the alkaline solution increases with concentration of the solute (Alonso, Gismera, Blanco, Lanzón, & Puertas, 2017; Varga, 2015). Therefore, increasing the viscosity is likely to decrease the workability of mortars in the fresh state.

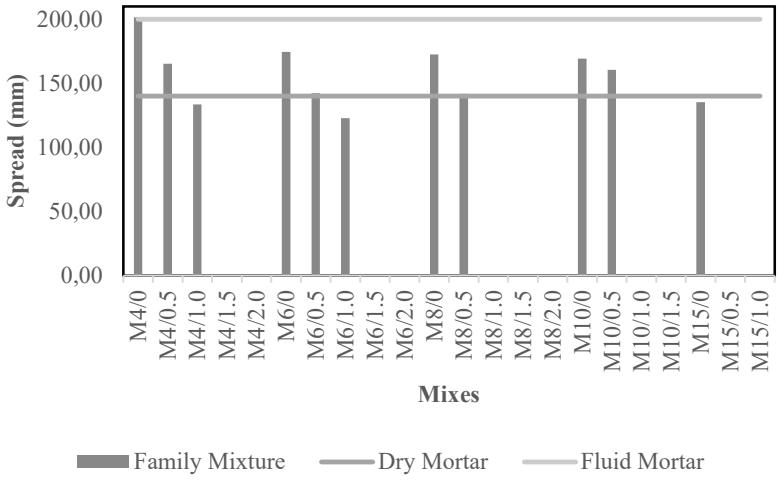

Figure 9 - Workability of MIBA mortars

(a) (b) (c)

Figure 10 - Slump flow result of (a) M4/M6 mixes, (b) M8/M10/M15 mixes and (c) M8/M10/M15 mixes 30 minutes later

FA mortars' workability presented a more stable behaviuor, since all mixes were classified as fluid, even though the amounts of NaOH and Na_2SiO_3 were the same for both types of precursor. The liquid/binder was higher in the research cited, since the alkaline solution prepared with the hydrated Na_2SiO_3, NaOH and water was considered as liquid, in which a plastic mortar could be obtained in a fresh state.

The phenomenon of loss of workability was probably minimized in FA mixes since the alkaline solution was prepared and immediately used for the manufacture of mortars, taking advantage of the heat of the reaction and therefore inhibiting a significant increase in apparent viscosity. According to the literature, previous studies reveal that, by increasing the temperature of the alkaline activator in the FA, the precipitation of the hydration products is enhanced (Palacios et al., 2019); therefore, the viscosity of the mix increases in the fresh state (Romagnoli, Leonelli, Kamse, & Lassinantti Gualtieri, 2012), but this was not observed in the present investigation.

3.4 Hardened-state performance

3.4.1 Compressive strength

3.4.1.1 Mortars with MIBA

Figure 11 shows the 28-day compressive strength results for all mortars made with MIBA. The maximum values were obtained by mortar M8/0, corresponding to 5.47MPa, and the lowest

values came from M4/0 at 0.87 MPa. The behaviour of the curve shows a trend in which it reaches a maximum value and then decreases for higher concentrations of Na_2O/binder, as well as a deterioration of the property when adding the sodium silicate solution.

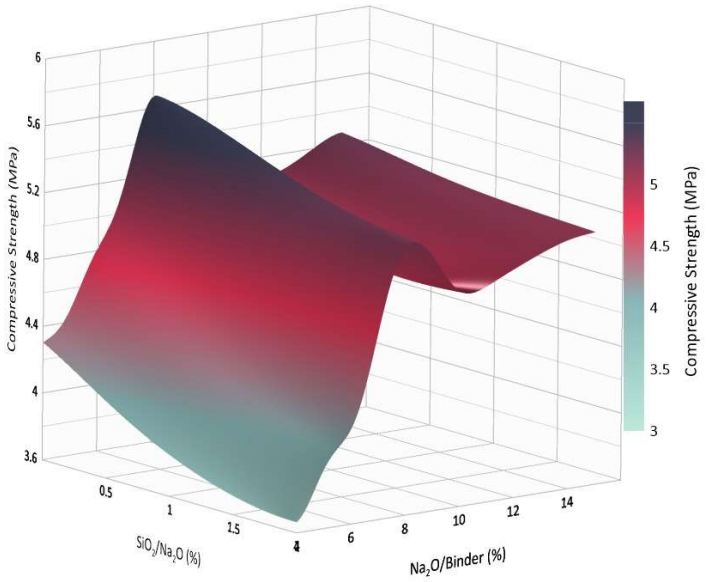

Figure 11 - Compressive strength of MIBA mortars

The effect of the Na_2O/binder ratio on the compressive strength of mortars is analysed from two perspectives: first, the one related to the effectiveness of the MIBA pretreatment before the manufacture of mortars, and the second from the characteristics of MIBA as a source of amorphous aluminosilicates available for dissolution in an alkaline medium.

Concerning the resting time, Huang et al. (2020) reported an improvement of the compressive strength of alkali-activated mortars using MIBA as precursor, by eliminating foaming and expansion, retaining the MIBA-NaOH solution for 3 hours before use, after which the compressive strength at 28 days was 8.4 MPa, while in the mortars that did not have this resting time it was 2.4 MPa. Therefore, the literature confirms the usefulness of this procedure, which in the present research lasted 24 hours.

The results of the influence of Na_2O/binder are in agreement with the literature. Huang et al. (2020) concluded that highly alkaline environments inhibit the formation and development of

activation products (i.e. C-(N-)A-S-H and N-A-S-H) and the excess Na^+ competes with active aluminium and active calcium, resulting in a decrease in compressive strength.

Regarding the second perspective related with the characteristics of MIBA as a source of amorphous aluminosilicates available for dissolution in an alkaline medium, the concentration of SiO_2 and Al_2O_3 available in MIBA, are lower than those available in FA. Therefore, the amount of amorphous phases will be lower. This greatly decreases the performance of the alkaline activation process, which is based on the dissolution of amorphous phases. The dissolution reactions of amorphous aluminosilicates that occur are generally the following (Kuenzel & Ranjbar, 2019):

$$Al_2O_3 + 3H_2O + OH^- \rightarrow 2Al(OH)_4^- \quad \text{Eq. 13}$$

$$SiO_2 + H_2O + OH^- \rightarrow [SiO(OH_3)]^- \quad \text{Eq. 14}$$

$$SiO_2 + 2OH^- \rightarrow [SiO_2(OH_2)]^{2-} \quad \text{Eq. 15}$$

Since the solubility of aluminosilicates depends on the amount of amorphous aluminosilicates available, as well as the hydroxyl ion concentration (Kuenzel & Ranjbar, 2019), it is necessary to quantify the amorphous contents available in MIBA to perform a more complete analysis of the results, including the role of Ca in the formation of gels. Likewise, large amounts of organic matter in MIBA, as non-incinerated material, decrease the availability of amorphous aluminosilicates.

In families with a Na_2O/binder greater than 10%, efflorescence was observed after 3 days of curing age (Figure 12). This indicates that excess Na^+ began to migrate to the surface through the interconnected porosity of the specimens and precipitated in the form of NaCl, Na_2CO_3 or $Na_3HCO_3CO_3 \cdot 2H_2O$. This phenomenon was also observed in the M8/1.5 and M8/2.0 families.

The influence of the ratio SiO_2/Na_2O on the compressive strength was found to be inversely proportional. This may have been due to the fact that, 24 hours after the pre-treatment of MIBA, the addition of sodium silicate led to a reaction with unoxidized aluminium, which produced a mix containing significant entrapped gas leading to a highly porous material. Such reaction has

been found to result in porous mortars with low thermal conductivity (Eliche-Quesada et al., 2020). Figure 13 shows the external view of mortars made with MIBA precursor.

Figure 12 - Efflorescence in MIBA mortars

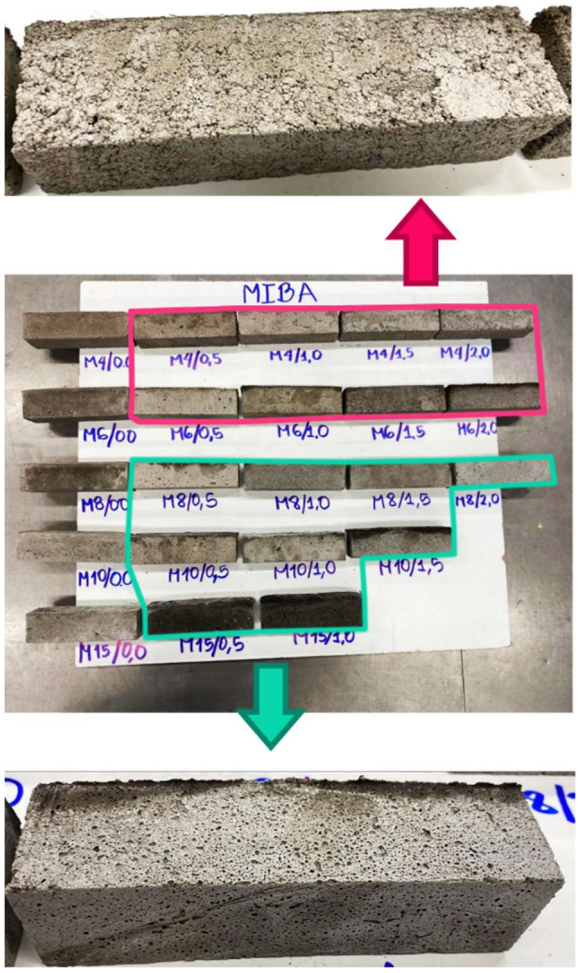

Figure 13 - External view of MIBA mortar

3.4.1.2 Mortars with FA

Figure 14 shows the 28-day compressive strength of mortars made with FA. The best result was obtained for mortar F15/1.0, corresponding to 50.66 MPa and the lowest result for F4/1.5 with 1.03 MPa. A clear trend was observed with increasing concentration of Na_2O/binder and SiO_2/Na_2O resulting in increased compressive strength. The alkaline activation of FA generally leads to a maximum value for an optimum content (Abdullah et al., 2011), after which it begins to exhibit a decline in performance, but that was not witnessed in the present investigation.

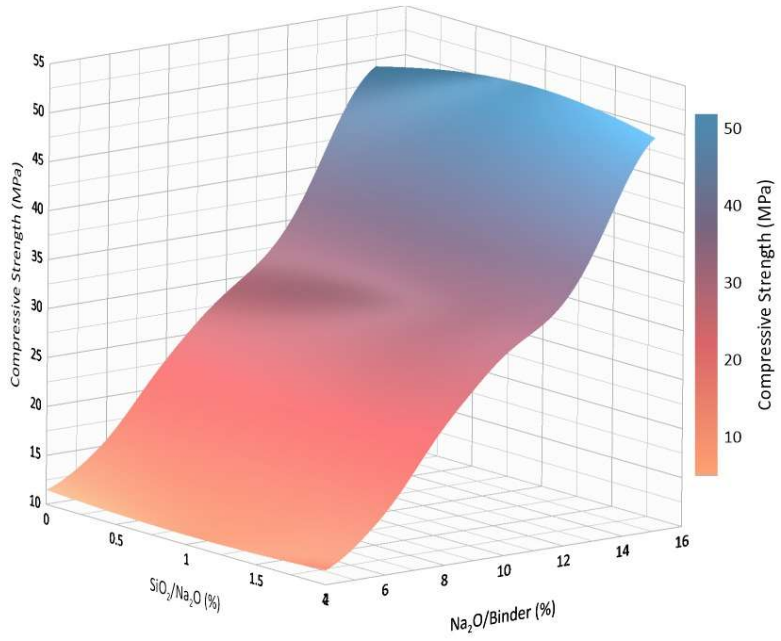

Figure 14 - Compressive strength of FA mortars

The amorphous phases of the aluminosilicates correspond to the reactive phases available for the activation process, which are directly associated with the efficiency of the combustion of coal and its composition. Silica structures available for this process correspond to the tetrahedral form of the $[SiO4]^{4-}$ ion, which forms tetrahedral chains that give rise to oligomers (Shekhovtsova et al., 2018). Na_2O/binder is directly related to the amount of OH^- ions present in the alkaline activator available to react with the binder. By increasing this ratio, the degree of dissolution of the aluminosilicates increases. For this reason, F15/0 presented the highest compressive strength development (19.99 MPa), a value 2.4 times higher than that of the F10/0

family. This behaviour is in accordance with what was found by various authors, where strength increases with the increase in OH^- concentration (Cho et al., 2017). Atis et al. (2015) varied the percentage of Na that came exclusively from NaOH, from 4% to 20%, finding that percentages greater than 16% decreased the compressive strength for curing temperatures above 75 °C (the average compressive strength was 45 MPa). For these concentrations, the gel produced corresponds to C-(N-)A-S-H and N-A-S-H (Djobo et al., 2016). Since Ca^{2+} is insolubilized in highly alkaline environments, it is probable that when the concentration of OH^- is exceeded, the compressive strength will decrease. In the present investigation, however, the threshold was not reached.

In Figure 14, it is possible to infer that increasing the SiO_2/Na_2O ratio leads to increased compressive strength, since the Si^{4+} species added from the sodium silicate will generate greater Si-O-Si bridges. The results suggest an optimum SiO_2/Na_2O ratio near 1.0, but additional testing would be required to confirm this. In the families F4/0.5, F6/0.5 and F8/0.5, the effect is opposite to what was expected, since the compressive strength is lower after 28 days than for F4/0, F6/0 and F8/0, respectively. Some researchers (Singh & Subramaniam, 2017) concluded that the compressive strength increases with increasing SiO_2/Na_2O ratio, which is in agreement with the present investigation. Figure 15 shows the visual appearance of the families made with FA.

Figure 15 - Visual appearance of FA mortars

Increasing the SiO_2/Na_2O ratio had a clear influence on the mortar's colour (white tonality), due to the presence of efflorescence. This is due to the migration of Na ions to the surface of the specimens, where their reaction with atmospheric CO_2 resulted in the precipitation of sodium carbonate species.

3.4.1.3 Compressive strength variation over time

Figure 16 shows the compressive strength of mortars M4, M6 versus F4 and F6 at 7, 14, 28, 91 and 182 days. For all M4 mixes and F4/0, a decline in compressive strength was observed, contrary to the trend observed in the mixes M6, F6 and the rest of the F4 mixes, in which a maximum compression strength was observed at 28 days, stabilizing henceforth.

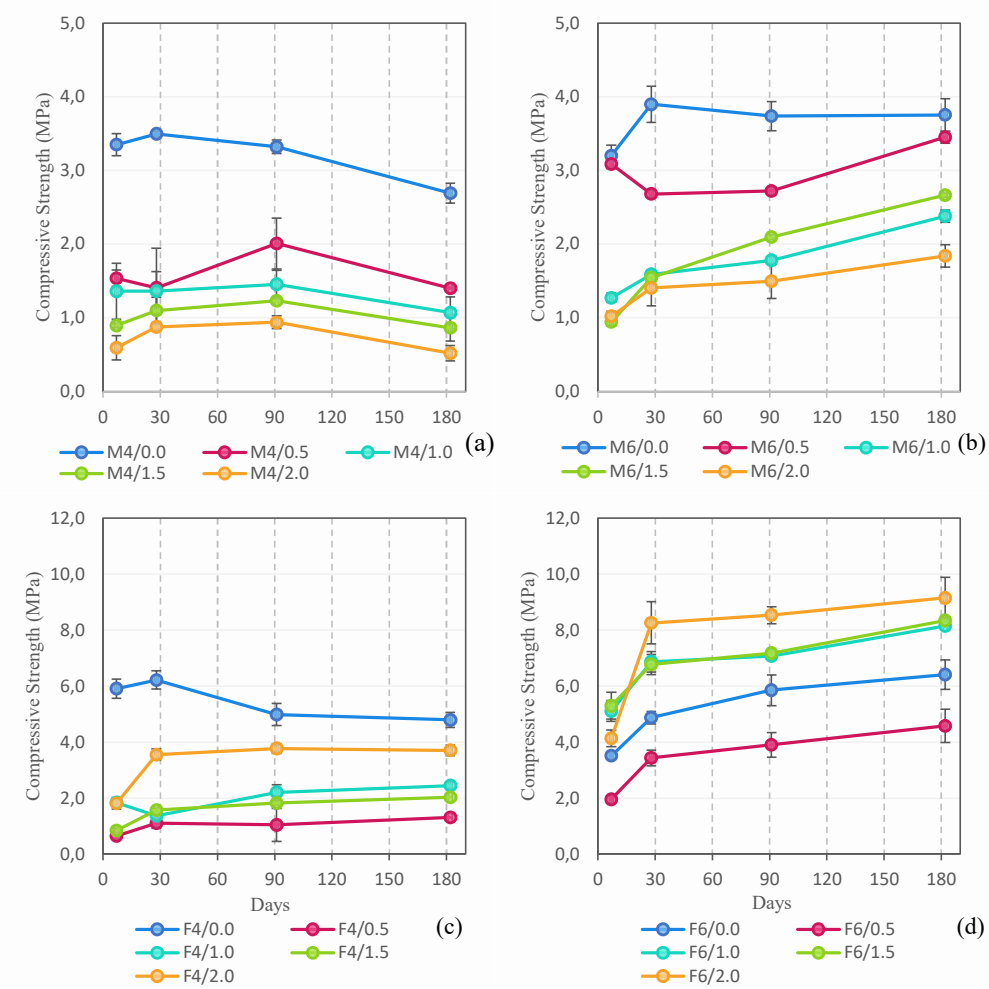

Figure 16 - Compressive strength vs. curing age for mixes M4 (a), M6 (b), F4 (c), F6 (d)

This behavior of the M4 mix could be related to the decrease in the hydroxyl ions (OH^-) available in the pretreatment stage (decrease when the Na_2SiO_3 content increases) (see Figure 5). Regarding the F4/0 mix, since the alkaline activator contained less NaOH than in other mixes, a lower pH level was attained and thus lower dissolution of amorphous aluminosilicate phases. The dry curing environment could be the cause of microcracks that resulted in a decrease in compressive strength over time.

Figure 17 shows the compressive strength of mortars M8 (a), M10 (b) and M15 (c) versus F8 (d), F10 (e), F15 (f) at 7, 14, 28, 91 and 182 days. In most of mixes an increase in compressive strength was observed with curing age, until reaching a maximum value at 28 days of curing. Mixes F10 and F15 with Na_2O content over 8% showed a significant increase in compressive strength when sodium silicate was added, contrary to what happens with mixtures made with MIBA. It is likely that this is due to the addition of Na_2SiO_3 only after the pretreament stage, in which the amount of water is significantly reduced with increasing SiO_2/Na_2O content thereby resulting in lower volumetric ratio of pretreatment solution/binder and thus less reacted aluminium particles.

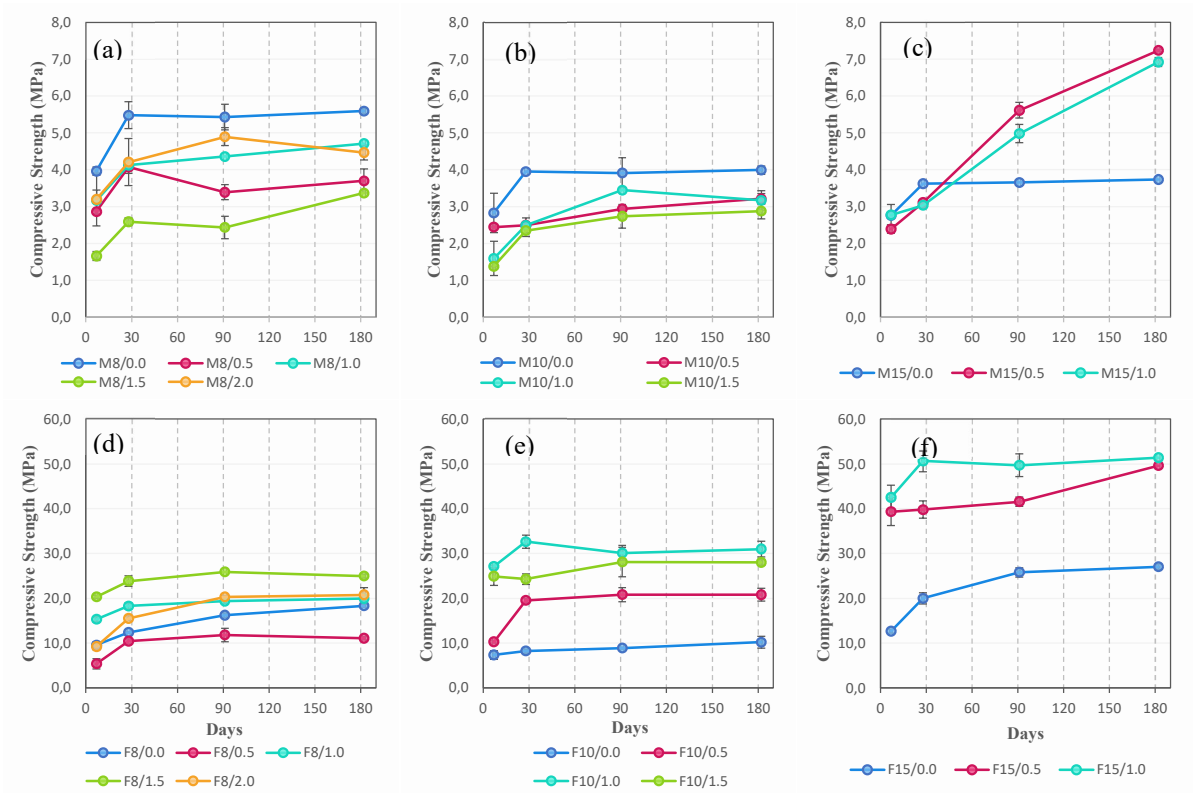

Figure 17 - Compressive strength vs. curing age for mixes M8 (a), M10 (b), M15 (c), F8 (d), F10 (e), F15 (f)

F15/0.5, F15/1.0, M15/0, M15/0.5 and M15/1.0 mortars showed an increase in compressive strength with increasing curing age over at 28 days, this is probably related to the formation of new reaction products (C-(N-)A-S-H and N-A-S-H) at late ages. Adesanya et al. (Adesanya, Ohenoja, Luukkonen, Kinnunen, & Illikainen, 2018) showed an improvement in compressive strength after 28 days of curing. The authors explained this behavior to be a result of the late release of Ca^{+} ions in the curing period, which takes place when $CaCO_3$ dissociates due to the decrease in pH in mortars and allowing the formation of new reaction products. Although M15/0.5 and M15/1.0 mixes reached compressive strengths higher than the M8/0 mix at 182 days, these mixes presented high efflorescence as shown in Figure 18. Table A and Table D**Error! Reference source not found.Error! Reference source not found.Error! Reference source not found.Error! Reference source not found.Error! Reference source not found.Error! Reference source not found.**show all the compressive strength results over time for MIBA and FA.

(a) (b)

Figure 18 - Efflorescence in mortars M15/0.5 (a) and M15/1.0 (b)

3.4.2 Flexural strength

3.4.2.1 MIBA mortars

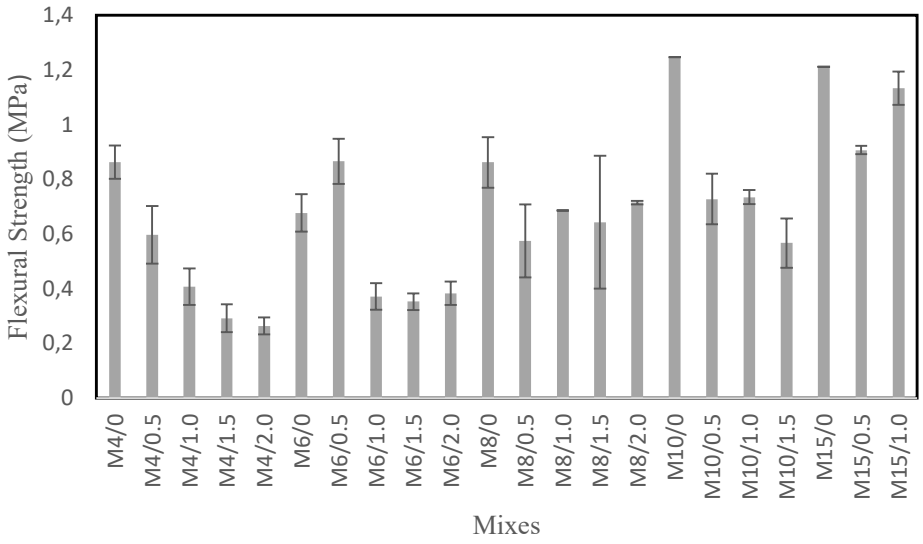

Figure 19 shows the 28-day flexural strength results for all mortars made with MIBA. The maximum values were obtained by mortar M10/0, corresponding to 1.247 MPa, and the lowest values came from M4/2.0 at 0.264 MPa. The behavior of the figure shows a trend in which by increasing the Na_2O content, the flexural strength increases, presenting a deterioration of the property when adding the sodium silicate solution. This behavior is associated with what is mentioned in chapter 3.4.1.1. Table B shows the flexural strength results over time for MIBA with the standard desviations values.

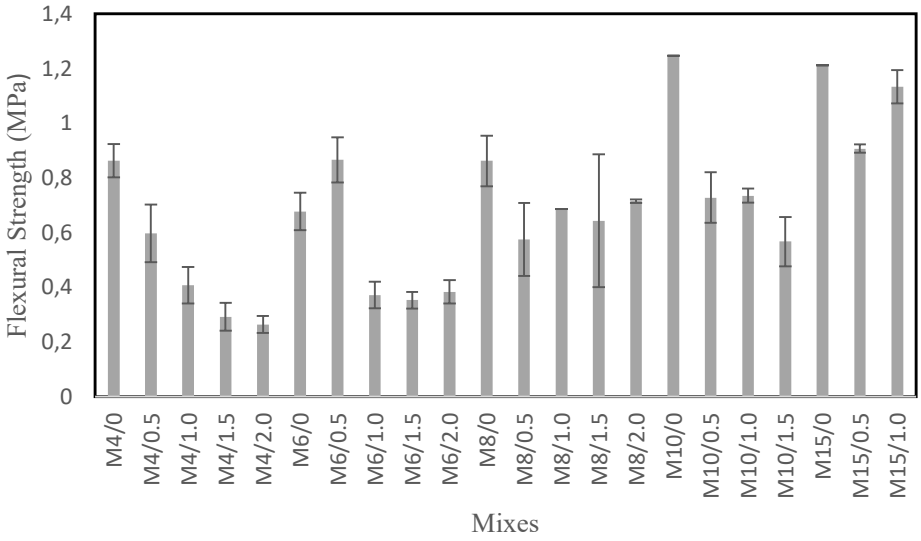

Figure 19 - Flexural strength of MIBA mortars

3.4.2.2 FA mortars

Figure 20 shows the 28-day flexural strength of mortars made with FA. The best result was obtained for mortar F15/1.0, corresponding to 9.44 MPa and the lowest result for F4/0.5 with 0.608 MPa. A clear trend was observed with increasing concentration of Na_2O/binder and SiO_2/Na_2O resulting in increased flexural strength. The alkaline activation of FA generally leads to a maximum value for an optimum content (Abdullah et al., 2011), after which it tipically begins to exhibit a decline in performance, but that was not witnessed in the present investigation. The associated behavior of the figure is explained in chapter 3.4.1.2. Table E shows all the conpressive strength results over time for MIBA and FA with the standard desviations values.

3.4.3 Dynamic modulus of elasticity

3.4.3.1 MIBA mortars

Figure 21 shows the 28-day moduli of elasticity for all mortars made with MIBA. The maximum values were obtained by mortar M8/0, corresponding to 6.252 GPa, and the lowest values came from M4/0 at 1.253 GPa. The behaviour of the curve shows a trend in which it reaches a maximum value and then decreases for higher concentrations of Na_2O/binder, as well

as a deterioration of the property when adding the Na_2SiO_3 solution. The modulus of elasticity of MIBA appears to vary directly with the compressive strength, since the Figure 11 and Figure 21 show a similar trend.

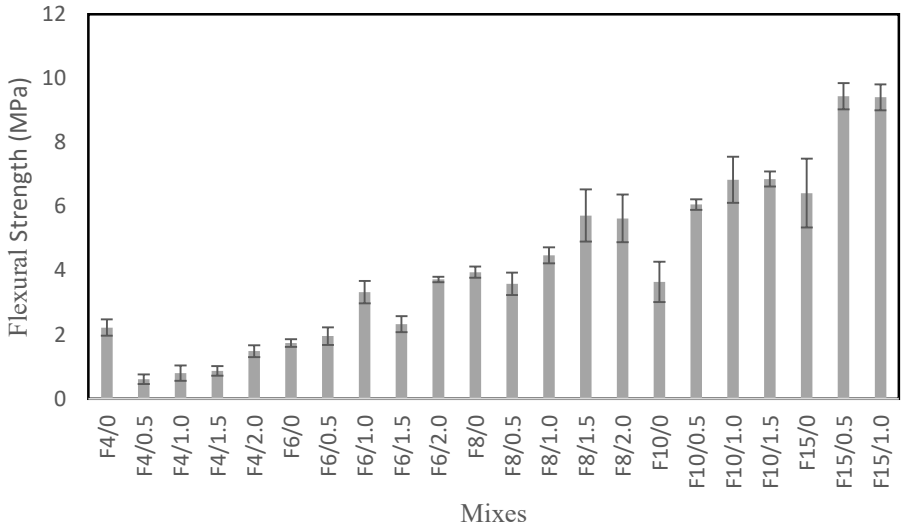

Figure 20 - Flexural strength of FA mortars

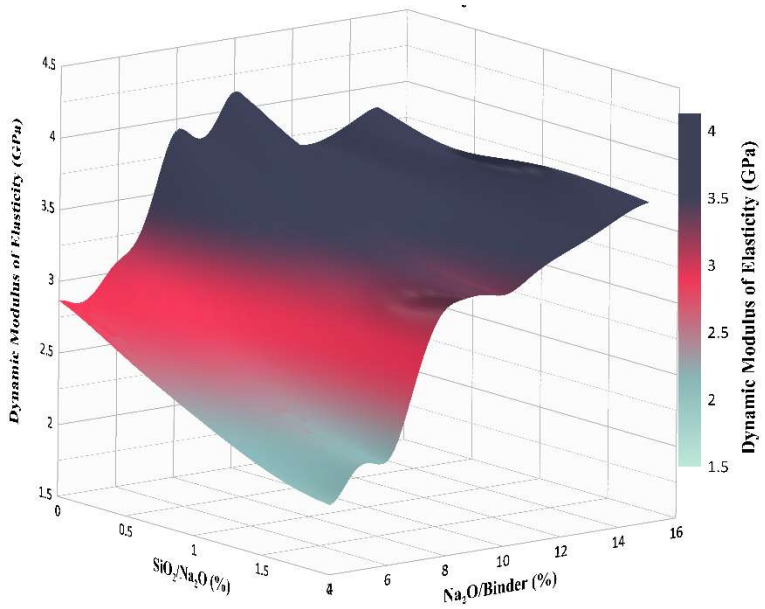

Figure 21 - Dynamic modulus of elasticity of MIBA mortars

A low modulus of elasticity is associated with a high porosity of the material, as well as a low degree of compaction and with the presence of microcracking, which indicates that mixes made

with MIBA possibly present these microstructural characteristics, that cause a decline in the elastic region (Coppola, Coffetti, & Crotti, 2018).

Figure 22 shows the linear correlation between the modulus of elasticity and the compressive strength. The R^2 obtained corresponds to 0.6982, showing that although the figures of compressive strength and modulus of elasticity both properties show similar trends, the linear adjustment does not fully explain the dependence between these properties. Table C shows the dynamic modulus of elasticity results over time for MIBA.

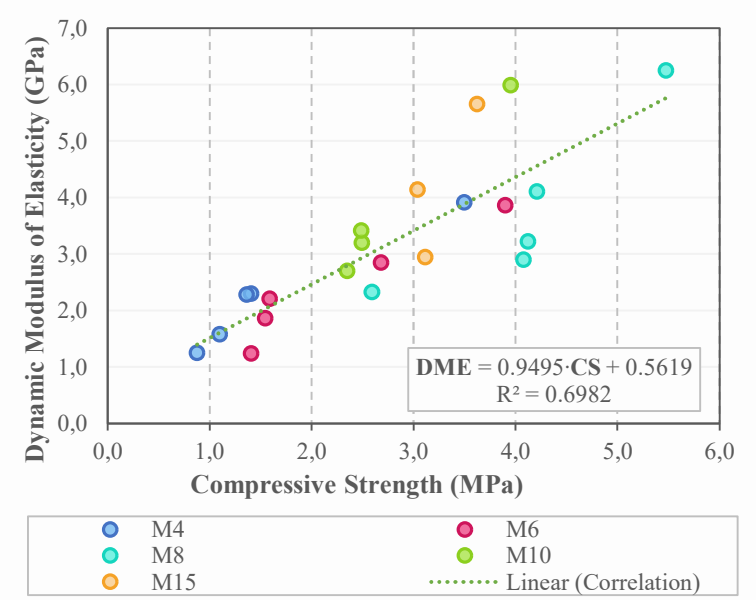

Figure 22 - Linear correlation compressive strength vs. modulus of elasticity of MIBA mixes

3.4.3.2 FA mortars

Figure 23 shows the 28-day moduli of elasticity for all FA mortars. The maximum values were obtained by mortar F15/1.0, corresponding to 24.8 GPa, and the lowest values came from F4/1.5 at 4.1 GPa. A clear trend was observed with increasing concentration of Na_2O/binder and SiO_2/Na_2O resulting in increased modulus of elasticity. Nath et al.(Nath & Sarker, 2017) in their research, evaluated the modulus of elasticity of alkali-activated concrete mixes, using type F FA as precursor and a solution of NaOH and Na_2SiO_3 as alkaline activator. They reported 28-day values in the range of 21.6-23.2 GPa, which is comparable to that in this

research for the same alkaline activator concentrations.

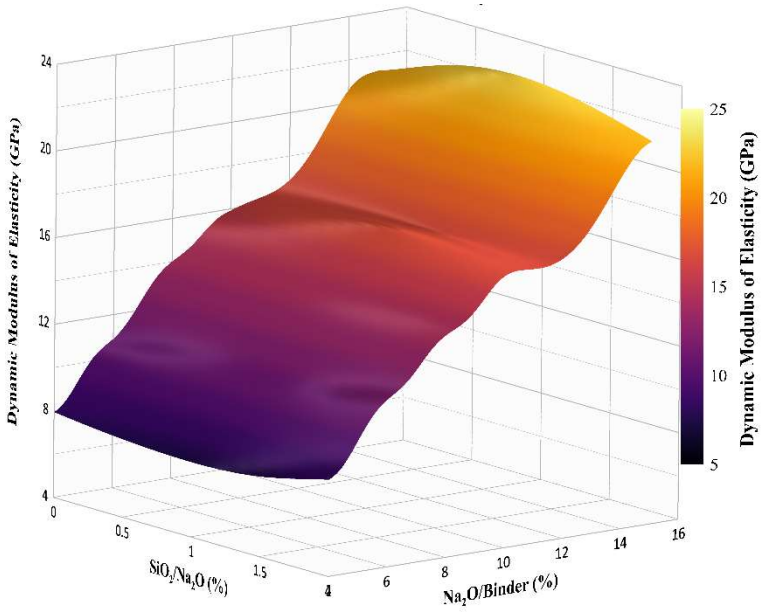

Figure 23 - Dynamic modulus of elasticity of FA mortars

The modulus of elasticity of FA mortars can be correlated with the compressive strength, since the Figure 14 and Figure 23 show a similar trend. Figure 24 presents the linear correlation between the modulus of elasticity and the compressive strength.

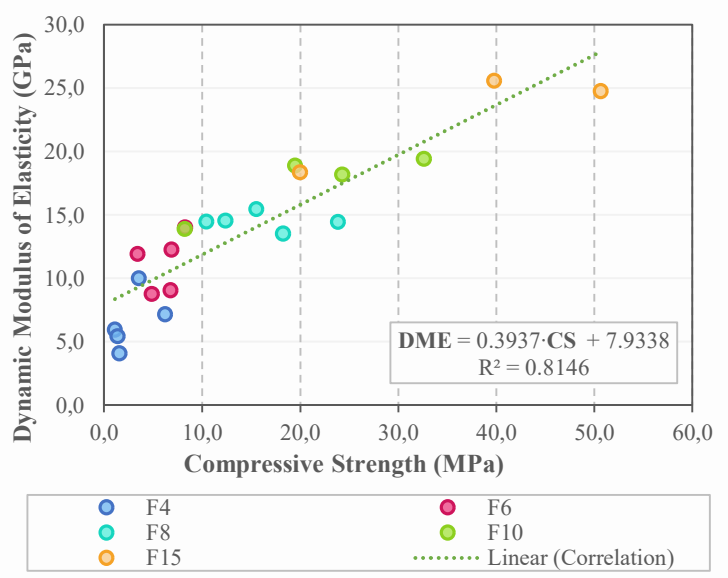

Figure 24 - Linear correlation compressive strength *vs*. modulus of elasticity for FA

The R^2 obtained corresponds to 0.8146, showing that although the figures of compressive strength and modulus of elasticity show similar trends, the linear adjustment does not fully explain the dependence between these properties. Table F shows the dynamic modulus of elasticity results over time of FA mortars.

4 Conclusions

From the previous results it is possible to conclude that:

- The chemical and mineralogical characterization of MIBA shows it does have some potential to be activated, but the high aluminium content is problematic in alkali-activated materials.
- The pretreatment was effective at reducing the amount of pure aluminium available to react thereby allowing the production of mortars with adequate dimensional stability.
- FA mortars were all very workable, to a point that hindered measuring the slump flow. It is recommended that the water/precursor ratio is reduced in future experimental campaigns.
- A resting time of 24 hours allowed the stabilization of the MIBA in the manufacturing process and thermal curing of AAM, but did not inhibit the reaction of the remaining aluminium with the Na_2SiO_3 solution added later on. This leads to an increase in internal porosity due to the increased production of H_2 gas, while affecting the workability of the mix in a fresh state.
- M8/0 and F15/1.0 mixes presented the best mechanical results at 28 days. Therefore, it is recommended the development of new mix designs from the combination of these precursors, seeking the highest possible MIBA content within a minimum strength loss scenario.
- The 28-day dynamic modulus of elasticity presented a similar trend as that of the compressive strength for both precursors, though with little linear adjustment.

Acknowledgements

The authors acknowledge the support of the CERIS Research Institute, IST, University of Lisbon and FCT- Foundation for Science and Technology, through the research project PTDC/ECI- CON/29196/2017 "Recycled Inorganic Polymer Concrete: Towards a fully recycled and cement-free concrete" (RInoPolyCrete). The authors would also like to acknowledge the support of Valorsul, EDP and SIKA for part of the materials provided for this experimental campaign.

References

Abdullah, M. M. A. B., Kamarudin, H., Abdulkareem, O. A., Ruzaidi, C., & Razak, R. (2011). *The effect of alkaline activator ratio on the compressive strength of fly ash-based geopolymers* (Vol. 5).

Adesanya, E., Ohenoja, K., Luukkonen, T., Kinnunen, P., & Illikainen, M. (2018). One-part geopolymer cement from slag and pretreated paper sludge. *Journal of Cleaner Production, 185*, 168-175. doi:10.1016/j.jclepro.2018.03.007

Alonso, M., Gismera, S., Blanco, M., Lanzón, M., & Puertas, F. (2017). Alkali-activated mortars: Workability and rheological behaviour. *Construction and Building Materials, 145*, 576-587.

Atis, C. D., Gorur, E. B., Karahan, O., Bilim, C., Ilkentapar, S., & Luga, E. (2015). Very high strength (120 MPa) class F fly ash geopolymer mortar activated at different NaOH amount, heat curing temperature and heat curing duration. *Construction and Building Materials, 96*, 673-678. doi:10.1016/j.conbuildmat.2015.08.089

Bayuseno, A. P., & Schmahl, W. W. (2010). Understanding the chemical and mineralogical properties of the inorganic portion of MSWI bottom ash. *Waste Management, 30*(8-9), 1509-1520. doi:10.1016/j.wasman.2010.03.010

Blasenbauer, D., Huber, F., Lederer, J., Quina, M. J., Blanc-Biscarat, D., Bogush, A., . . . Dahlbo, H. (2020). Legal situation and current practice of waste incineration bottom ash utilisation in Europe. *Waste Management, 102*, 868-883.

Bocullo, V., Vaičiukynienė, D., Gečys, R., & Daukšys, M. (2020). Effect of Ordinary Portland Cement and Water Glass on the Properties of Alkali Activated Fly Ash Concrete. *Minerals, 10*(1), 40.

BS EN 1015-3 Determination of consistence of fresh mortar (by flow table). (1999).

Coppola, L., Coffetti, D., & Crotti, E. (2018). Pre-packed alkali activated cement-free mortars for repair of existing masonry buildings and concrete structures. *Construction and*

Building Materials, 173, 111-117. doi:https://doi.org/10.1016/j.conbuildmat.2018.04.034

Cristelo, N., Segadães, L., Coelho, J., Chaves, B., Sousa, N. R., & de Lurdes Lopes, M. (2020). Recycling municipal solid waste incineration slag and fly ash as precursors in low-range alkaline cements. *Waste Management, 104*, 60-73.

Cho, Y. K., Yoo, S. W., Jung, S. H., Lee, K. M., & Kwon, S. J. (2017). Effect of Na2O content, SiO2/Na2O molar ratio, and curing conditions on the compressive strength of FA-based geopolymer. *Construction and Building Materials, 145*, 253-260. doi:10.1016/j.conbuildmat.2017.04.004

Djobo, J. N. Y., Tchakoute, H. K., Ranjbar, N., Elimbi, A., Tchadjie, L. N., & Njopwouo, D. (2016). Gel Composition and Strength Properties of Alkali-Activated Oyster Shell-Volcanic Ash: Effect of Synthesis Conditions. *Journal of the American Ceramic Society, 99*(9), 3159-3166. doi:10.1111/jace.14332

Eliche-Quesada, D., Ruiz-Molina, S., Pérez-Villarejo, L., Castro, E., & Sánchez-Soto, P. J. (2020). Dust filter of secondary aluminium industry as raw material of geopolymer foams. *Journal of Building Engineering*, 101656. doi:https://doi.org/10.1016/j.jobe.2020.101656

EN, B. (1999). BS EN 1015-6: Determination of bulk density of fresh mortar *1015-6*.

Engineering ToolBox. Hydrogen - Density and Specific Weight. (2018). Retrieved 07/06/2019

Fang, G. H., Ho, W. K., Tu, W. L., & Zhang, M. Z. (2018). Workability and mechanical properties of alkali-activated fly ash-slag concrete cured at ambient temperature. *Construction and Building Materials, 172*, 476-487. doi:10.1016/j.conbuildmat.2018.04.008

Farhan, N. A., Sheikh, M. N., & Hadi, M. N. S. (2019). Investigation of engineering properties of normal and high strength fly ash based geopolymer and alkali-activated slag concrete compared to ordinary Portland cement concrete. *Construction and Building Materials, 196*, 26-42. doi:10.1016/j.conbuildmat.2018.11.083

Hoppe Filho, J. (2017). Atividade pozolânica de adições minerais para cimento Portland (Parte I): Índice de atividade pozolânica (IAP) com cal, difração de raios-X (DRX), termogravimetria (TG/DTG) e Chapelle modificado. *Revista Materia, 22*(3).

Huang, G., Ji, Y., Li, J., Zhang, L., Liu, X., & Liu, B. (2019). Effect of activated silica on polymerization mechanism and strength development of MSWI bottom ash alkali-activated mortars. *Construction and Building Materials, 201*, 90-99. doi:10.1016/j.conbuildmat.2018.12.125

Huang, G., Ji, Y., Zhang, L., Li, J., & Hou, Z. (2018). The influence of curing methods on the strength of MSWI bottom ash-based alkali-activated mortars: The role of leaching of OH^- and free alkali. *Construction and Building Materials, 186*, 978-985. doi:https://doi.org/10.1016/j.conbuildmat.2018.07.224

Huang, G., Yang, K., Chen, L., Lu, Z., Sun, Y., Zhang, X., . . . Xu, Z. (2020). Use of pretreatment to prevent expansion and foaming in high-performance MSWI bottom ash alkali-activated mortars. *Construction and Building Materials, 245*, 118471. doi:https://doi.org/10.1016/j.conbuildmat.2020.118471

Huang, G., Yang, K., Sun, Y., Lu, Z., Zhang, X., Zuo, L., . . . Xu, Z. (2020). Influence of NaOH content on the alkali conversion mechanism in MSWI bottom ash alkali-activated mortars. *Construction and Building Materials, 248*, 118582. doi:https://doi.org/10.1016/j.conbuildmat.2020.118582

Khale, D., & Chaudhary, R. (2007). Mechanism of geopolymerization and factors influencing its development: a review. *Journal of Materials Science, 42*(3), 729-746. doi:10.1007/s10853-006-0401-4

Kim, J., An, J., Nam, B. H., & Tasneem, K. M. (2016). Investigation on the side effects of municipal solid waste incineration ashes when used as mineral addition in cement-based material. *Road Materials and Pavement Design, 17*(2), 345-364. doi:10.1080/14680629.2015.1083463

Kuenzel, C., & Ranjbar, N. (2019). Dissolution mechanism of fly ash to quantify the reactive aluminosilicates in geopolymerisation. *Resources, Conservation and Recycling, 150*, 104421. doi:https://doi.org/10.1016/j.resconrec.2019.104421

Liu, Y., Sidhu, K. S., Chen, Z., & Yang, E.-H. (2018). Alkali-treated incineration bottom ash as supplementary cementitious materials. *Construction and Building Materials, 179*, 371-378. doi:https://doi.org/10.1016/j.conbuildmat.2018.05.231

Lothenbach, B., Scrivener, K., & Hooton, R. (2011). Supplementary cementitious materials. *Cement and Concrete Research, 41*(12), 1244-1256.

Lynn, C. J., Dhir, R. K., & Ghataora, G. S. (2017). Municipal incinerated bottom ash use as a cement component in concrete. *Magazine of Concrete Research, 69*(10), 512-525.

Maldonado-Alameda, A., Giro-Paloma, J., Svobodova-Sedlackova, A., Formosa, J., & Chimenos, J. M. (2020). Municipal solid waste incineration bottom ash as alkali-activated cement precursor depending on particle size. *Journal of Cleaner Production, 242*, 118443. doi:https://doi.org/10.1016/j.jclepro.2019.118443

Mary Joseph, A., Snellings, R., Nielsen, P., Matthys, S., & De Belie, N. (2020). Pre-treatment and utilisation of municipal solid waste incineration bottom ashes towards a circular economy. *Construction and Building Materials, 260*, 120485. doi:https://doi.org/10.1016/j.conbuildmat.2020.120485

Materials, A. S. o. T. (2017). Standard Specification for Coal Fly Ash and Raw or Calcined Natural Pozzolan for Use in Concrete.

Materials, A. S. o. T. (2019). Standard Test Methods for pH of Soils (pp. 6).

Myers, R. J., Bernal, S. A., & Provis, J. L. (2014). A thermodynamic model for C-(N-)A-S-H gel: CNASH_ss. Derivation and validation. *Cement and Concrete Research, 66*, 27-47. doi:10.1016/j.cemconres.2014.07.005

Nath, P., & Sarker, P. K. (2017). Flexural strength and elastic modulus of ambient-cured blended low-calcium fly ash geopolymer concrete. *Construction and Building Materials, 130*, 22-31. doi:https://doi.org/10.1016/j.conbuildmat.2016.11.034

Palacios, M., Alonso, M. M., Varga, C., & Puertas, F. (2019). Influence of the alkaline solution and temperature on the rheology and reactivity of alkali-activated fly ash pastes. *Cement & Concrete Composites, 95*, 277-284. doi:10.1016/j.cemconcomp.2018.08.010

Puertas, F., Varga, C., & Alonso, M. (2014). Rheology of alkali-activated slag pastes. Effect of the nature and concentration of the activating solution. *Cement and Concrete Composites, 53*, 279-288.

Rashad, A. M., & Zeedan, S. R. (2011). The effect of activator concentration on the residual strength of alkali-activated fly ash pastes subjected to thermal load. *Construction and Building Materials, 25*(7), 3098-3107. doi:https://doi.org/10.1016/j.conbuildmat.2010.12.044

Raverdy, M., Brivot, F., Paillere, A., & Dron, R. (1980). Appréciation de l'activité pouzzolanique de constituents secondaires. *Proceedings of 7e congrés international de la chimie des ciments, Paris, France*, 6-41.

Romagnoli, M., Leonelli, C., Kamse, E., & Lassinantti Gualtieri, M. (2012). Rheology of geopolymer by DOE approach. *Construction and Building Materials, 36*, 251-258. doi:https://doi.org/10.1016/j.conbuildmat.2012.04.122

Rosenband, V., & Gany, A. (2010). Application of activated aluminum powder for generation of hydrogen from water. *International Journal of Hydrogen Energy, 35*(20), 10898-10904. doi:https://doi.org/10.1016/j.ijhydene.2010.07.019

Shekhovtsova, J., Zhernovsky, I., Kovtun, M., Kozhukhova, N., Zhernovskaya, I., & Kearsley, E. (2018). Estimation of fly ash reactivity for use in alkali-activated cements - A step towards sustainable building material and waste utilization. *Journal of Cleaner Production, 178*, 22-33. doi:10.1016/j.jclepro.2017.12.270

Singh, G., & Subramaniam, K. V. L. (2017). Evaluation of sodium content and sodium hydroxide molarity on compressive strength of alkali activated low-calcium fly ash. *Cement & Concrete Composites, 81*, 122-132. doi:10.1016/j.cemconcomp.2017.05.001

Técnicas, A.-A. B. d. N. (2010). NBR 15895. Materiais pozolânicos – Determinação do teor de hidróxido de cálcio fixado – Método Chapelle modificado (pp. 6).

Tian, X., Rao, F., León-Patiño, C. A., & Song, S. (2020). Effects of aluminum on the expansion and microstructure of alkali-activated MSWI fly ash-based pastes. *Chemosphere, 240*, 124986.

Varga, C. (2015). Cementos activados alcalinamente: Comportamiento reológico y durable en medio ácido. *PhD Tesis, UNED Madrid, Spain*.

Wei, Y., Saffarzadeh, A., Shimaoka, T., Zhao, C., Peng, X., & Gao, J. (2014). Geoenvironmental weathering/deterioration of landfilled MSWI-BA glass. *Journal of Hazardous materials, 278*, 610-619. doi:10.1016/j.jhazmat.2014.05.093

Xuan, D., Tang, P., & Poon, C. S. (2018). Limitations and quality upgrading techniques for utilization of MSW incineration bottom ash in engineering applications – A review. *Construction and Building Materials, 190*, 1091-1102. doi:https://doi.org/10.1016/j.conbuildmat.2018.09.174

Appendix

Table A - Compressive strength of MIBA mortars

Mix	Age (days)							
	7		28		91		182	
	Avg. (MPa)	STD (MPa)	Avg. (MPa)	STD (MPa)	Avg. (MPa)	STD (MPa)	Avg. (MPa)	STD (MPa)
M4/0	3.350	0.150	3.496	0.041	3.320	0.091	2.692	0.135
M4/0.5	1.538	0.110	1.408	0.536	2.008	0.343	1.402	0.011
M4/1.0	1.361	0.382	1.364	0.264	1.455	0.192	1.070	0.214
M4/1.5	0.895	0.029	1.100	0.181	1.233	0.011	0.866	0.181
M4/2.0	0.594	0.168	0.877	0.051	0.939	0.086	0.520	0.104
M6/0	3.198	0.144	3.898	0.245	3.738	0.199	3.753	0.221
M6/0.5	3.086	0.020	2.680	0.315	2.720	0.550	3.450	0.247
M6/1.0	1.272	0.062	1.589	0.044	1.780	0.055	2.380	0.082
M6/1.5	0.944	0.053	1.545	0.085	2.095	0.029	2.664	0.029
M6/2.0	1.022	0.066	1.406	0.244	1.498	0.236	1.841	0.150
M8/0	3.963	0.115	5.477	0.367	5.430	0.347	5.591	0.071
M8/0.5	2.864	0.133	4.077	0.180	3.391	0.208	3.695	0.325
M8/1.0	3.167	0.285	4.122	0.279	4.361	0.388	4.709	0.247
M8/1.5	1.661	0.122	2.591	0.103	2.436	0.303	3.369	0.133
M8/2.0	3.195	0.717	4.209	0.637	4.897	0.243	4.469	0.199
M10/0	2.830	0.537	3.951	0.287	3.914	0.409	3.991	0.115
M10/0.5	2.447	0.022	2.493	0.197	2.939	0.055	3.208	0.139
M10/1.0	1.592	0.462	2.489	0.086	3.447	0.004	3.169	0.265
M10/1.5	1.377	0.011	2.351	0.162	2.736	0.325	2.877	0.210
M15/0	2.762	0.173	3.623	0.073	9.160	0.044	8.110	0.269
M15/0.5	2.391	0.110	3.113	0.035	5.614	0.214	7.236	0.029
M15/1.0	2.777	0.276	3.038	0.077	4.981	0.243	6.919	0.119

Table B - Flexural strength of MIBA mortars

Mix	Age							
	7		28		91		182	
	Avg. (MPa)	STD (MPa)	Avg. (MPa)	STD (MPa)	Avg. (MPa)	STD (MPa)	Avg. (MPa)	STD (MPa)
M4/0	0.879	0.003	0.863	0.061	0.834	0.013	0.800	0.018
M4/0.5	0.523	0.043	0.597	0.105	0.640	0.076	0.595	0.046
M4/1.0	0.448	0.036	0.407	0.067	0.396	0.003	0.305	0.050
M4/1.5	0.189	0.001	0.292	0.051	0.332	0.035	0.389	0.063
M4/2.0	0.143	0.053	0.264	0.031	0.232	0.056	0.173	0.050
M6/0	0.693	0.012	0.677	0.068	0.661	0.083	0.544	0.083
M6/0.5	0.764	0.017	0.866	0.082	0.809	0.050	0.907	0.003
M6/1.0	0.313	0.041	0.372	0.048	0.398	0.076	0.485	0.023
M6/1.5	0.238	0.022	0.353	0.030	0.594	0.015	0.645	0.027
M6/2.0	0.266	0.022	0.383	0.043	0.416	0.048	0.575	0.008
M8/0	0.721	0.031	0.862	0.093	1.078	0.116	1.059	0.056
M8/0.5	0.633	0.066	0.575	0.133	0.553	0.087	0.492	0.027
M8/1.0	0.550	0.065	0.686	0.099	0.725	-	0.943	0.099
M8/1.5	0.543	0.118	0.643	0.243	0.614	0.060	0.816	-
M8/2.0	0.588	0.018	0.715	0.007	1.009	0.051	0.964	0.008
M10/0	1.048	0.020	1.247	-	1.287	0.146	1.301	0.070
M10/0.5	0.623	0.013	0.728	0.093	0.792	0.103	0.932	0.008
M10/1.0	0.571	0.045	0.735	0.026	0.996	0.003	1.249	0.129
M10/1.5	0.340	0.007	0.567	0.090	0.694	0.073	0.854	0.078
M15/0	0.935	0.060	1.211	0.077	1.756	-	1.616	-
M15/0.5	0.731	0.007	0.907	0.015	1.322	0.043	2.141	0.227
M15/1.0	0.976	0.025	1.134	0.061	1.877	0.169	2.019	0.121

Table C - Dynamic modulus of elasticity for MIBA mortars

Mix	Age							
	7		28		91		182	
	Avg. (GPa)	STD (MPa)	Avg. (GPa)	STD (MPa)	Avg. (GPa)	STD (MPa)	Avg. (GPa)	STD (MPa)
M4/0	4.131	0.199	3.915	0.652	4.272	0.237	4.076	0.676
M4/0.5	2.393	0.368	2.296	0.202	3.347	0.234	2.606	0.168
M4/1.0	1.573	0.832	2.282	0.297	2.444	0.119	1.969	0.512
M4/1.5	1.078	0.214	1.580	0.021	1.915	0.083	2.012	0.350
M4/2.0	0.725	0.373	1.253	0.007	1.327	0.110	1.065	0.119
M6/0	4.198	0.286	3.862	0.359	4.331	0.288	4.024	0.061
M6/0.5	2.377	0.145	2.849	0.410	3.467	0.987	3.858	0.476
M6/1.0	1.512	0.075	2.205	0.307	2.531	0.528	2.555	0.240
M6/1.5	1.102	0.211	1.864	0.229	2.486	0.011	2.730	0.270
M6/2.0	1.189	0.072	1.238	0.282	1.656	0.082	2.182	0.014
M8/0	3.876	0.670	6.252	0.218	5.632	1.919	4.632	0.585
M8/0.5	3.433	0.156	2.897	0.236	2.546	0.041	2.726	0.069
M8/1.0	2.545	0.046	3.219	0.097	3.157	0.048	3.654	0.055
M8/1.5	1.472	0.316	2.325	0.291	2.507	0.309	2.649	0.144
M8/2.0	2.781	0.408	4.103	0.393	3.802	1.024	5.941	0.225
M10/0	5.199	0.297	5.991	0.251	5.984	0.550	5.601	0.839
M10/0.5	2.656	0.475	3.199	0.456	4.139	0.059	4.062	0.153
M10/1.0	2.320	0.232	3.413	0.084	4.254	0.328	4.557	0.020
M10/1.5	1.623	0.103	2.701	0.120	3.332	0.169	3.691	0.187
M15/0	3.799	0.092	5.655	0.262	5.853	1.096	5.687	0.496
M15/0.5	1.999	0.123	2.941	0.303	5.504	0.109	7.433	0.063
M15/1.0	3.575	0.126	4.141	0.372	7.871	0.299	7.889	0.153

Table D - Compressive strength for FA mortars

Mix	Age							
	7		28		91		182	
	Avg. (MPa)	STD (MPa)	Avg. (MPa)	STD (MPa)	Avg. (MPa)	STD (MPa)	Avg. (MPa)	STD (MPa)
F4/0	5.908	0.343	6.219	0.325	4.984	0.393	4.792	0.267
F4/0.5	0.652	0.117	1.103	0.184	1.044	0.597	1.313	0.424
F4/1.0	1.841	0.013	1.370	0.116	2.205	0.276	2.447	0.133
F4/1.5	0.842	0.073	1.573	0.070	1.825	0.066	2.031	0.150
F4/2.0	1.814	0.201	3.552	0.198	3.770	0.175	3.705	0.188
F6/0	3.508	0.117	4.875	0.225	5.856	0.548	6.413	0.526
F6/0.5	1.955	0.122	3.436	0.280	3.905	0.436	4.579	0.865
F6/1.0	5.111	0.369	6.869	0.367	7.075	0.106	8.152	0.011
F6/1.5	5.297	0.482	6.776	0.361	7.177	0.069	8.345	0.060
F6/2.0	4.136	0.298	8.260	0.756	8.539	0.303	9.152	0.731
F8/0	9.545	0.736	12.380	0.155	16.214	0.488	18.322	0.283
F8/0.5	5.369	1.158	10.419	0.547	11.811	1.478	11.092	0.369
F8/1.0	15.316	0.583	18.259	0.708	19.341	0.495	19.944	0.124
F8/1.5	20.295	0.329	23.849	1.158	25.900	0.004	24.953	0.402
F8/2.0	9.223	0.709	15.514	0.545	20.303	0.393	20.764	1.589
F10/0	7.347	0.981	8.225	0.461	8.894	0.208	10.197	1.313
F10/0.5	10.272	0.252	19.496	0.455	20.802	1.545	20.792	1.430
F10/1.0	27.117	0.289	32.628	1.511	30.095	1.735	30.978	1.768
F10/1.5	24.925	2.029	24.280	1.178	28.102	3.308	28.022	0.650
F15/0	12.681	0.415	19.992	1.260	25.806	1.061	27.033	0.603
F15/0.5	39.331	3.094	39.794	1.928	41.589	1.019	49.611	0.749
F15/1.0	42.514	2.764	50.664	2.463	49.700	2.519	51.413	5.913

Table E - Flexural strength for FA mortars

Mix	Age							
	7		28		91		182	
	Avg. (MPa)	STD (MPa)	Avg. (MPa)	STD (MPa)	Avg. (MPa)	STD (MPa)	Avg. (MPa)	STD (MPa)
F4/0	1.300	0.088	2.221	0.255	2.568	0.022	2.332	0.129
F4/0.5	0.671	0.171	0.608	0.149	0.289	0.108	0.769	-
F4/1.0	0.416	0.008	0.799	0.240	1.061	0.005	1.126	0.088
F4/1.5	0.722	0.060	0.870	0.146	1.168	0.202	1.587	-
F4/2.0	1.507	0.010	1.486	0.186	1.382	0.191	1.488	0.030
F6/0	1.506	0.075	1.739	0.123	2.303	0.081	2.175	0.066
F6/0.5	1.084	0.005	1.954	0.274	2.086	0.380	2.617	0.132
F6/1.0	1.773	0.247	3.327	0.345	3.500	0.061	3.025	0.187
F6/1.5	2.040	0.456	2.328	0.251	2.447	0.020	2.562	0.855
F6/2.0	1.952	0.176	3.723	0.083	3.768	0.234	4.147	0.399
F8/0	3.489	0.041	3.950	0.176	5.273	0.703	5.141	0.061
F8/0.5	2.248	0.136	3.588	0.349	3.664	0.098	3.336	0.452
F8/1.0	3.342	0.206	4.472	0.249	4.705	0.164	5.141	0.290
F8/1.5	2.950	0.141	5.718	0.817	6.891	0.189	6.955	0.552
F8/2.0	4.425	0.653	5.628	0.741	5.728	0.136	5.148	0.124
F10/0	2.861	0.038	3.645	0.627	3.475	0.081	4.373	0.166
F10/0.5	2.766	0.133	6.059	0.168	5.749	0.149	5.307	0.423
F10/1.0	5.378	0.204	6.833	0.718	7.129	0.297	8.128	-
F10/1.5	4.978	0.464	6.857	0.237	6.655	0.055	8.252	-
F15/0	3.384	0.540	6.415	1.073	6.652	0.723	9.238	0.704
F15/0.5	8.406	0.144	9.440	0.412	12.530	0.563	11.531	0.113
F15/1.0	8.374	0.063	9.405	0.409	12.587	0.572	11.586	0.234

Table F - Dynamic modulus of elasticity of FA mortars

Mix	Age							
	7		28		91		182	
	Avg. (GPa)	STD (MPa)	Avg. (GPa)	STD (MPa)	Avg. (GPa)	STD (MPa)	Avg. (GPa)	STD (MPa)
F4/0	7.666	0.192	7.174	0.481	7.014	0.645	7.061	1.378
F4/0.5	3.148	0.104	5.947	0.335	6.380	0.226	5.637	0.623
F4/1.0	3.731	0.056	5.456	0.612	6.882	0.537	7.850	1.439
F4/1.5	3.395	0.036	4.084	2.507	7.652	0.014	9.113	0.313
F4/2.0	5.722	0.245	10.013	0.241	11.884	0.009	12.017	0.370
F6/0	6.685	0.148	8.766	0.698	11.387	0.770	17.205	1.322
F6/0.5	5.266	0.872	11.927	0.640	11.738	0.787	12.981	1.491
F6/1.0	9.044	0.338	12.274	0.580	13.579	0.294	15.632	0.189
F6/1.5	6.971	0.454	9.068	0.585	8.811	0.076	10.067	0.794
F6/2.0	6.510	0.278	14.020	0.391	14.158	0.678	15.523	1.141
F8/0	14.313	2.391	14.549	0.468	15.698	0.506	16.253	0.470
F8/0.5	9.732	0.388	14.486	0.407	15.133	0.136	15.882	0.097
F8/1.0	11.103	0.929	13.533	0.260	14.311	0.479	14.984	0.275
F8/1.5	12.380	0.129	14.451	0.493	15.497	0.081	16.382	0.345
F8/2.0	7.762	0.291	15.472	0.352	18.943	0.040	20.322	0.848
F10/0	10.524	1.761	13.886	0.332	14.804	0.829	15.448	0.577
F10/0.5	12.601	0.355	18.883	1.868	20.711	0.626	20.766	0.383
F10/1.0	16.491	1.096	19.429	0.109	20.182	0.183	21.402	0.579
F10/1.5	14.627	1.048	18.198	0.323	20.671	0.540	21.779	0.905
F15/0	13.445	1.718	18.371	5.123	24.995	0.855	19.555	0.827
F15/0.5	20.459	6.223	25.584	0.139	30.996	0.234	31.150	0.086
F15/1.0	24.394	0.398	24.758	1.223	30.187	1.016	29.507	0.459

Lisboa, 31/03/2021

Authors

Yoleimy Ávila Pereira	Rui Vasco Silva
PhD Candidate	PhD Researcher

Jorge de Brito

Full Professor